Supplementary Information

Development of Multifunctional Liquid-infused Materials by Printing Assisted Functionalization on Porous Nanocomposites

Wenqing He [a], Peng Liu [a], Jieke Jiang [a], Meijin Liu [a], Hualin Li [a], Jianqiang Zhang [a], Yan Luo[b], Hon Yeung Cheung [a] and Xi Yao *[ac]

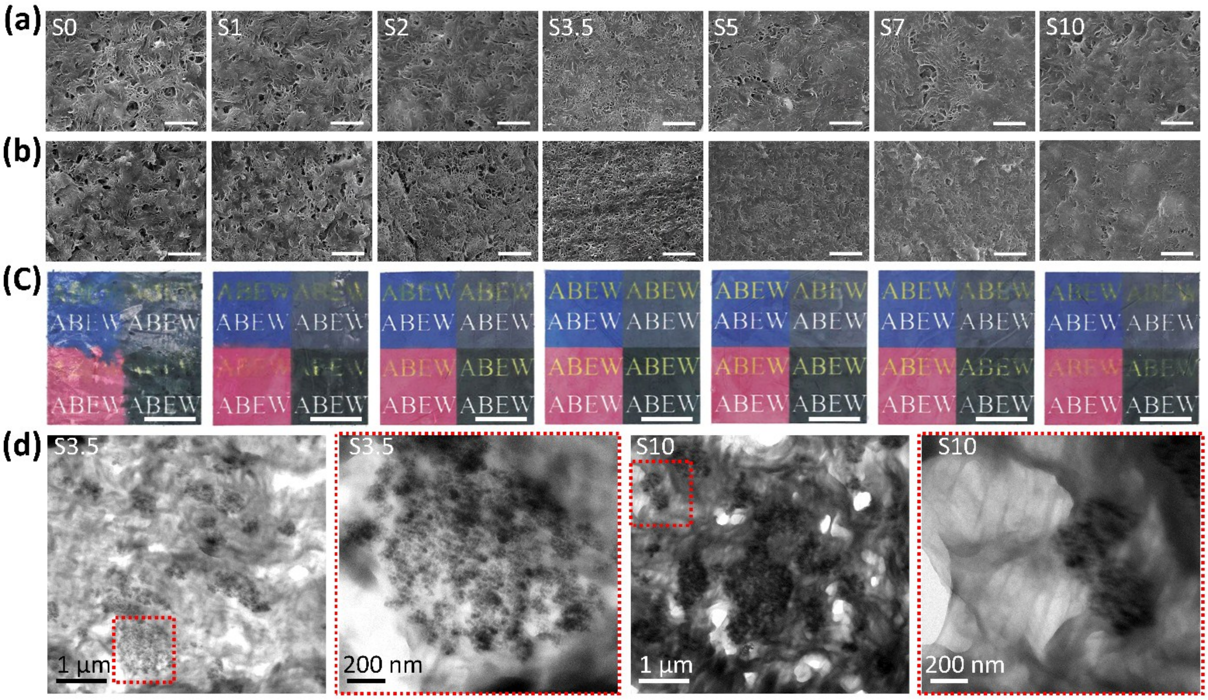

Fig. S1 SEM images showing the morphology of top surface (a) and cross-section (b) of UHMWPE/SiO_2 nanocomposites with various SiO_2 content. (c) Optical imaging showing the ink-jet printing performance on corresponding UHMWPE/SiO_2 nanocomposites. Four character "ABEW" with four kinds of background colors were printed. (d) Cross-section TEM images of the nanocomposites S3.5 and S10. Scale bar: (a) and (b) 5 μm; (c) 1 cm.

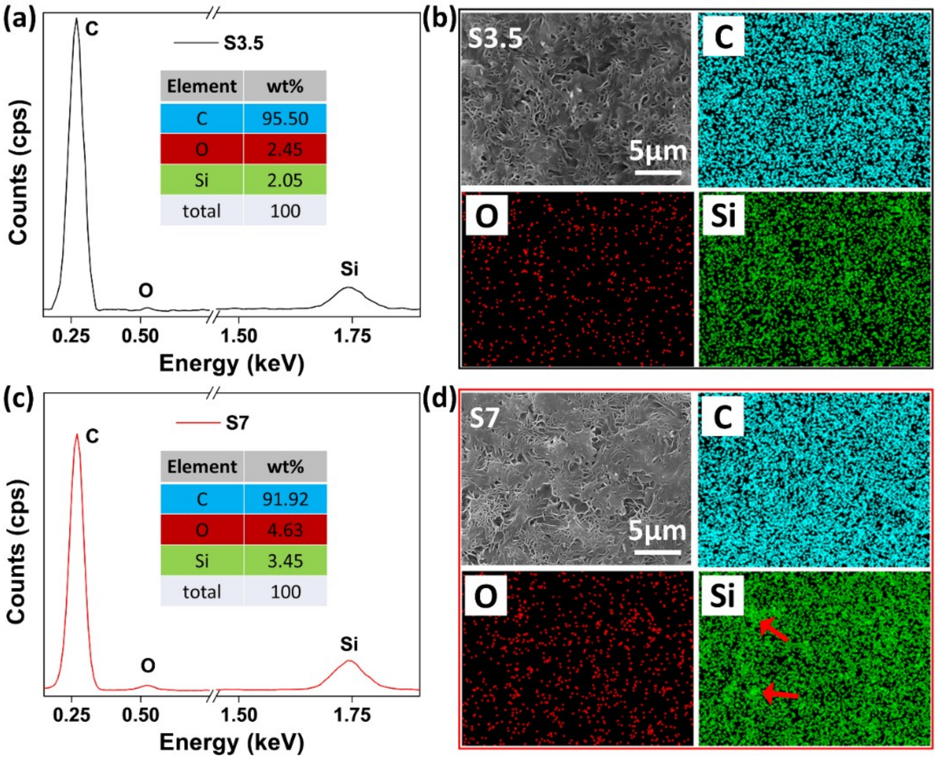

Fig. S2 (a) EDS analysis of UHMWPE/SiO_2 nanocomposite (S3.5). (b) The corresponding SEM and EDS mapping image of S3.5. (c) EDS analysis of UHMWPE/SiO_2 nanocomposite (S7) (d) The corresponding SEM and EDS mapping image of S7. The green spots marked with red arrows indicated the phase-separation induced severe agglomeration of SiO_2 on S7.

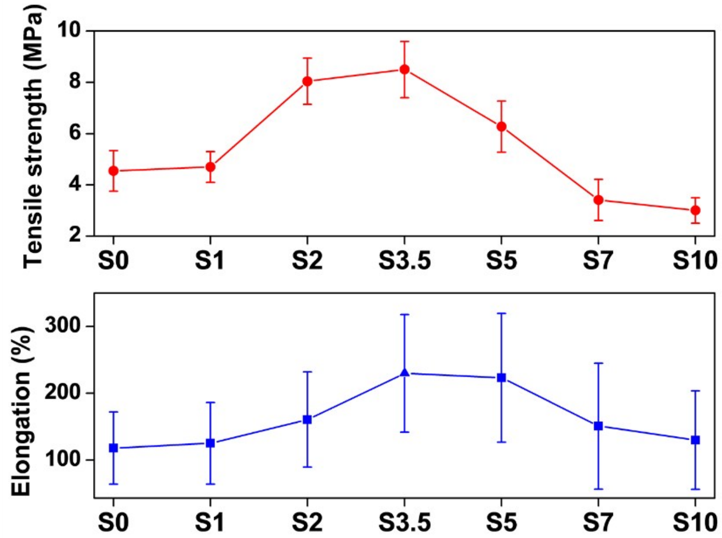

Fig. S3 Tensile property of UHMWPE/SiO_2 nanocomposite SN. The addition of SiO_2 nanoparticles could improve the tensile strength of the nanocomposite, while the severe agglomeration of excessive SiO_2 will deteriorate the tensile property of nanocomposite.

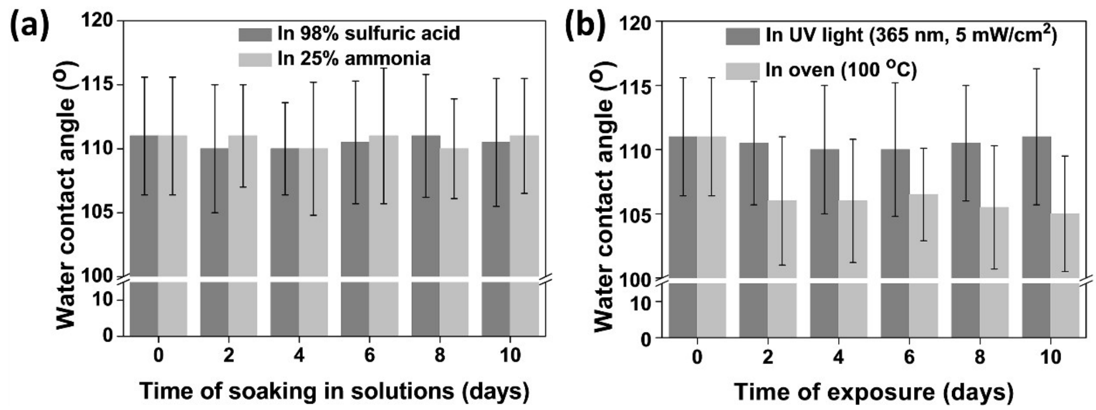

Fig. S4 Stability tests of the UHMWPE/SiO_2 nanocomposite. Variation of the water contact angle on the typical printable nanocomposite S3.5 sustained in acid and base solutions (a) and exposed in UV light (365 nm, 5 mW/cm^2) and in oven (100 ^oC). The surface hydrophobicity was unaffected and water contact angle was maintained around 110° under above treatments.

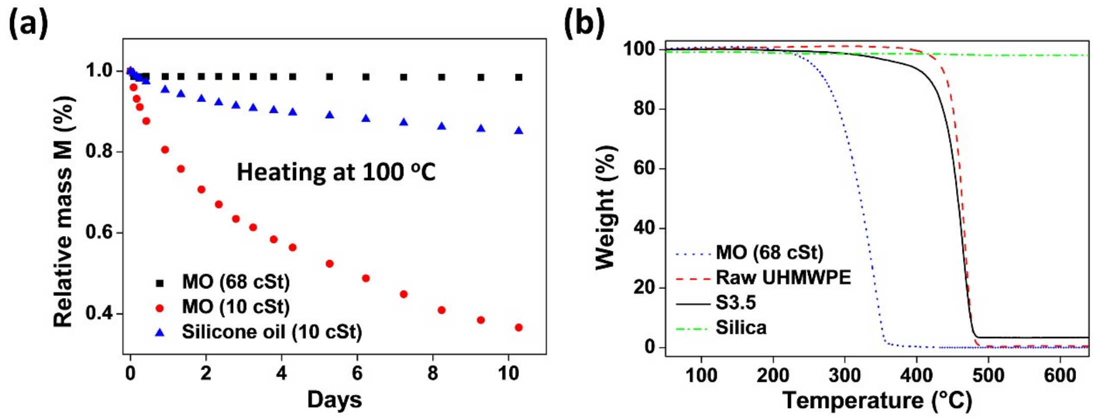

Fig. S5 (a) Evaporation characteristics of three kinds of fluorine-free lubricants. (b) Thermogravimetric analysis (TGA) of S3.5 and raw materials, including UHMWPE, mineral oil and SiO_2. The 68 cSt mineral oil showed minimal evaporation rate and high decomposition temperature (around 230 °C), and brought high thermal stability to the lubricated sample as showed in Figure 2c.

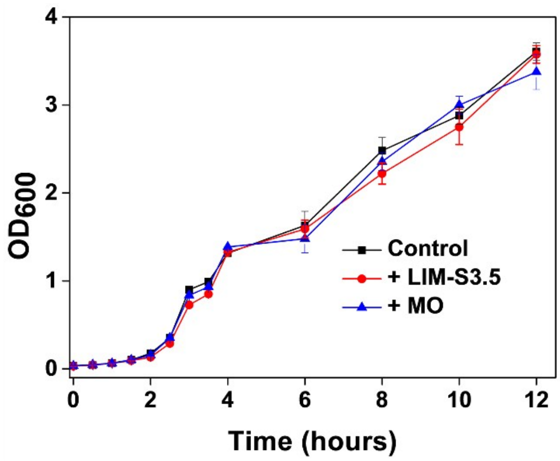

Fig. S6 Indistinguishable growth curves of *P. aeruginosa* cultured in shaken L-B media containing mineral oil and LIM-S3.5, comparing to control group. Both mineral oil and LIM-S3.5 showed no inhibition on *P. aeruginosa* growth. Thus, the non-adhesion of bacteria on LIM-S3.5 was attributed to the mineral oil layer worked as a slippery interface between nanocomposite and bacteria.

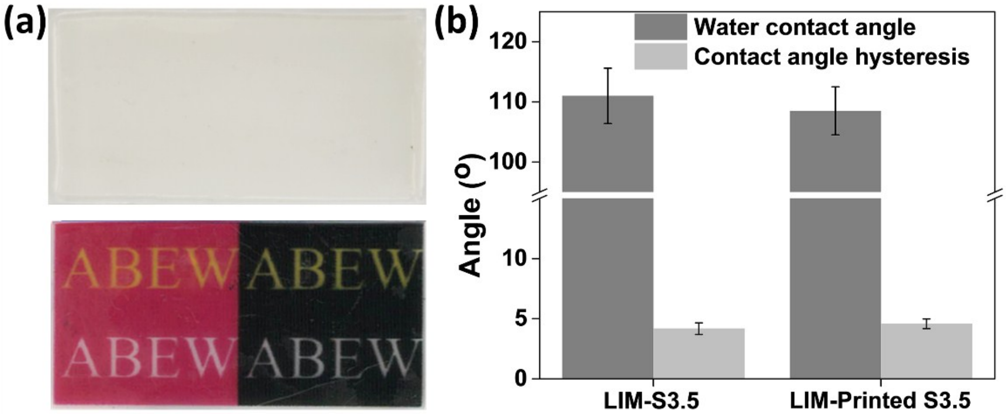

Fig. S7 The LIM-Printed-S3.5 demonstrated almost the same slippery property of LIM-S3.5. (a) LIM-S3.5 (up) and LIM-Printed S3.5 (bottom). (b) WCA and CAH of LIM-S3.5 and LIM-Printed S3.5. With CAH lower than 5°, the LIM-Printed S3.5 can keep surface slipperiness.

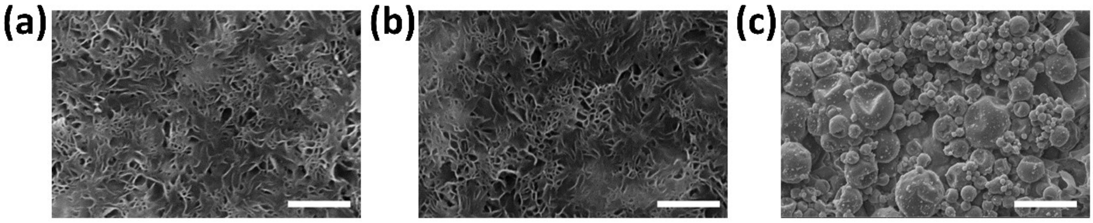

Fig. S8 Surface morphology of nanocomposite after printing with (a) commercial original ink (b) hydrochromic ink (35 g/m^2) (c) thermochromic ink. Comparing with nanocomposite without ink (See figure S1, S2), the effect of morphology changes caused by hydrochromic inks and original inks can be ignored. Thus, the retained oil layer got thinner was mainly caused by the reduced affinity between mineral oil and substrate (see Fig. 4a). Scale bar: 5 µm.

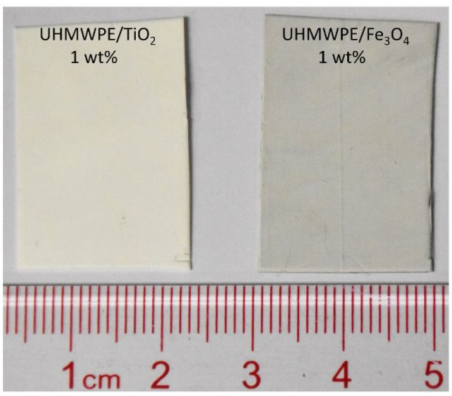

Fig. S9 Optical images of nanocomposites with different oxides. Left: UHMWPE/TiO_2, right: UHMWPE/Fe_3O_4. The whiteness of the two nanocomposites was different due to the distinct appearance of oxide particles.

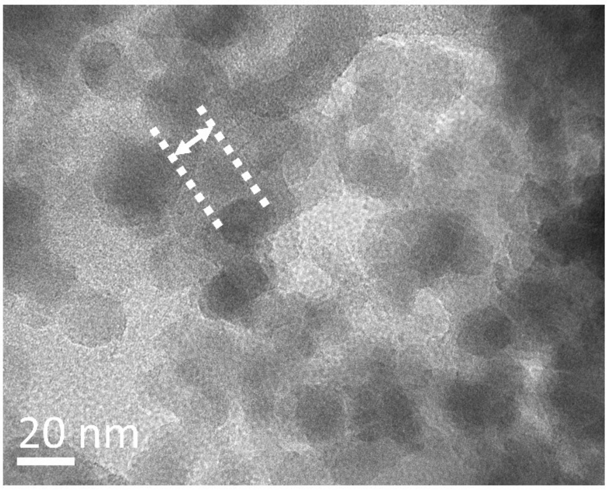

Fig. S10 The enlarged TEM image of nanocomposite S3.5 showing the primary particle size of SiO_2.